Title: **Experimental parameter sensitivity analysis of residual stresses induced by deep rolling on 7075-T6 aluminium alloy**

Authors: **M. Beghini, L. Bertini, B.D. Monelli, C. Santus, M. Bandini**

Experimental parameter sensitivity analysis of residual stresses induced by deep rolling on 7075-T6 aluminium alloy

M. Beghini[a], L. Bertini[a], B. Monelli[a], C. Santus[a,*], M. Bandini[b]

[a] *University of Pisa. DICI - Department of Civil and Industrial Engineering. Largo L. Lazzarino 2, 56122 Pisa, Italy.*
[b] *Peen Service Srl. Via A. Pollastri 7, 40138 Bologna, Italy.*

Abstract

The residual stress distribution induced by deep rolling depends on several factors: material elasto-plastic curve, roller shape, indentation force and rolling feed. Among these, the force and the feed are those parameters that can be easily handled without costs or layout modifications. This paper shows an experimental investigation about these two parameters and a comparative analysis on the obtained residual stress profiles. The deep rolling treatment was performed on aluminium alloy 7075-T6 samples and the used tool was a carbide roller with conical and rounded contact. The residual stresses were measured by combining the hole drilling method and the X-ray diffraction technique. A first evident result was the large difference between the two principal residual stress components. The feed direction residual stress was almost a factor of two larger than the rolling direction residual stress. Parameter trends on residual stress distributions were investigated. The depth of the compressive region increased with the rolling force and the maximum stress position also tended to be subsurface, while for lower loads the maxima were at the surface. On the other hand, the feed parameter did not produce any effect at large depth, and just the initial subsurface distribution was slightly influenced. Nevertheless, the surface hardness was noticeably affected by the feed, while the rolling force had a less predominant role. Finite element simulations were also carried out and reported in the paper, mainly to have information about induced work hardening. The plasticity depth was only affected by the load, indeed it was very similar to the compressive residual stress depth, while the maximum accumulated plasticity was significantly increased by the feed.

Keywords: Deep Rolling; Residual Stresses; Hole Drilling Method; X-Ray Diffraction; 7075-T6 aluminium alloy.

*Corresponding author: Ciro Santus
Ph. +39 (0)50 2218007, Fax +39 (0)50 2210604.
Email address: ciro.santus@ing.unipi.it (C. Santus)

Nomenclature

DR	Deep Rolling.
HDM	Hole Drilling Method.
XRD	X-Ray Diffraction.
FE	Finite Element method.
E	Young's modulus.
S_{Y}	Yield strength.
S_{U}	Ultimate tensile strength.
δ_{N}	Toolholder imposed normal displacement.
d_{R}	Residual indentation depth.
F_{N}	Normal force during deep rolling treatment, also referred to as rolling force.
$F_{\mathrm{N,av}}$	Average value of the normal force during deep rolling.
$F_{\mathrm{N,std}}$	Standard deviation of the normal force during deep rolling.
f	Rolling feed: the pitch between rolling subsequent traces.
α	Clearance angle: inclination of the rolling tool conical surface.
r_{R}	Fillet radius of the rolling tool.
R_{a}	Surface average roughness.
$\sigma_x, \sigma_y, \tau_{\mathrm{xy}}$	Residual stress components along generic directions.
$\sigma_{\mathrm{f}}, \sigma_{\mathrm{r}}, \tau_{\mathrm{fr}}$	Residual stress components along feed and rolling directions.
$\sigma_{\mathrm{f0}}, \sigma_{\mathrm{r0}}$	Residual stress components at the surface, feed and rolling directions.
$\sigma_{\mathrm{f,max}}, \sigma_{\mathrm{r,max}}$	Maximum residual stress components, feed and rolling components.
d_{c}	Depth of compressive residual stresses.
$d_{\mathrm{f,max}}, d_{\mathrm{r,max}}$	Maximum compressive residual stress depths, feed and rolling directions.
ε_{p}	Accumulated plastic strain after rolling.
$\varepsilon_{\mathrm{p,max}}$	Maximum of the accumulated plastic strain distribution.

1. Introduction

Mechanical treatments that produce plasticity deformation by means of a hard rolling indenter pushed against the surface of a ductile metal component can be categorized as: "Burnishing", "Low Plasticity Burnishing" and "Deep Rolling". Burnishing [1] is a treatment mainly dedicated to the surface finish enhancement and/or to the surface hardness improvement [2, 3, 4], where the plastic deformation is limited to the scale of surface roughness asperities. This treatment is not primarily dedicated to the induction of residual stresses. On the other hand Deep Rolling (DR) [5] (sometimes also referred to as "Deep Cold Rolling" [6], or "Deep Ball Burnishing" with the spherical indenter [7]) is a treatment basically designed for introducing surface and subsurface highly compressive residual stresses. In specific applications, DR can be limited to the notch radiused region, such as at shaft fillets [8, 9]. Otherwise the treatment can be performed under feed operation [10], following a setup comparable to burnishing, and merely using same tools, however with enhanced rolling forces. The surface finish improvement is still obtained even with DR, along with high cold working [6, 10, 11]. This latter surface effect can be beneficial as associated to the hardness improvement, but also detrimental since it is reason of material embrittlement [12, 13], these two controversial factors can have relative roles depending on the applied load and the specific material. Low plasticity burnishing, developed and patented by Lambda Technologies, also referred to as "Roller Burnishing" e.g. by the Ecoroll company and by Klocke and Liermann [14], or "Ball Burnishing" by López et al. [15], is both dedicated to surface roughness reduction and high and deep compressive residual stresses. The main difference, with respect to deep rolling, is that high residual stress is obtained with reduced work hardening [16, 17, 18], essentially due to the large size of the spherical indenter. This kind of burnishing is usually performed on common machine tools, with a hydrostatic bearing system for the ball roller that requires

a pressurization unit. Even complex geometries, such as impeller blades, can be treated by means of this technology [19, 20], but obviously there are limitations at notches due to the roller shape.
Besides burnishing and deep rolling, there are other techniques dedicated to the surface improvement, specifically for introducing residual stresses. Among these, Shot Peening is the most common [21, 22, 23]. This mechanical surface treatment is more flexible for different and complex geometries such as sharp notches [24, 25, 26]. Though the detrimental effect of surface roughness, severe work hardening, and limited depth of residual stresses [5, 16], the fatigue strength enhancement produced by shot peening still is remarkable. This can be attributed to the shallow depth of the fatigue "process volume", or the so called (fatigue) critical distance [27], that actually can be quite small for high strength structural alloys. For example, this size is smaller than 0.1 mm for 7xxx aluminium alloys and then completely inside the shot peening compressive depth, as well discussed by Benedetti et al. [24].
Parameter investigation is a crucial task for surface treatments. An accurate choice of parameters can give optimal performance, such as surface roughness or fatigue strength improvement, on the contrary the erratic selection of the treatment parameters can even be detrimental with respect to the untreated condition. About the burnishing process, a parameter investigation was performed by El-Axir [2]. He showed the effects on micro-hardness and surface roughness, and proposed empirical equations for the parameter dependencies. He found that the after treatment surface properties are dependent on force, number of passes, feed, and also rolling speed. El-Axir showed that the rolling speed indirectly produces an effect on burnishing due to tool chattering, also confirmed by El-Khabeery and El-Axir [28]. This effect can be reason of concern for high production rates, while it is not an issue for low speed rolling. Moreover, El-Axir showed that multiple passes cause material overhardening. As mentioned above about low plasticity burnishing, it is desirable to have surface improvements: low roughness and compressive residual stresses, just with a limited hardening to avoid embrittlement and also to have residual stress stability [12, 13, 17]. Small value of the feed produces remarkable results in terms of hardness and surface finish, however, similarly to multiple passes, severe work hardening of the material again results. Parametric analysis were also reported by Rodríguez et al. [7] showing the effects of the speed, the feed and the rolling load (here the load was the hydrostatic pressure for supporting the ball). They found that the optimum burnishing results are in the range $0.2 - 0.1$ µm in terms of final R_a, though "good enough" surface treatment can be considered when the roughness is less than 0.5 µm that is a typical value of the grinding process, thus the grinding itself could be replaced by the burnishing (or the deep rolling) as finishing. Moreover, they showed that the after burnishing roughness significantly depends on the previous surface roughness, this was also confirmed by Prabhu et al. [6, 10, 11] and also evident in the present study.
The present research investigated the residual stresses induced by deep rolling with a tool having a "conical and radiused shape". The literature is mainly dedicated on burnishing and deep rolling with the ball type indenter. Nevertheless, remarkable deep rolling results were obtained with this tool that has practical advantages with respect to the low plasticity burnishing. This roller shape can easily manage shouldered geometries, not accessible by the ball type indenter, moreover no external fluid pressurization unit is required to control the rolling load. Balland et al. [29] investigated a similar rolling tool, cylindrical and rounded, with the axis having a small inclination angle with respect to the specimen surface. The contact reduced to a small area with largely different curvatures, and consequently the residual stress components were quite different. More specifically, the component along the high curvature radius was remarkably higher than the other. This residual stress anisotropy, also well evident in the present study, is a quality rather than a shortcoming when the loading is mainly applied along a specific direction. E.g. a shaft under rotating bending fatigue has the cyclic normal stress direction aligned with the axis, thus the higher residual stress component along this axial direction generates a well dedicated fatigue crack prevention.
Finite Element (FE) simulation is a familiar tool for residual stress prediction. There is a large literature about modeling residual stresses produced by different industrial processes such as welding, heat treatment, machining, etc. (see the review paper by Mackerle [30]) and about surface plastic deformation processes, such as shot peening [22, 31, 32] and also deep rolling [7, 33, 34, 35, 36, 37, 38, 29, 39]. The main results of a literature review about low plasticity burnishing and deep rolling FE modeling can be summarized as follows:

- Plane strain simulation can be preferable rather than full 3D modeling. Though the unavoidable geome-

try simplification, in a plain model the element size can be remarkable reduced, especially at the initial subsurface region that experiences high stress gradients. The plane strain does not allow the material from flowing along the out-of-plane direction, however, the 3D cumbersome model reduces the modeled geometry to a very small portion of the specimen surface with evident limitations in terms of adequate boundary conditions.

- Final surface finish can be successfully modeled both with plane and 3D models. Also pre-existing surface roughness can be introduced in the FE model to reproduce more realistically the final surface texture.
- Residual stress distribution is usually considered as uniform along any direction parallel to the specimen surface, and stress gradient is just assumed along the depth. The cyclic indentation, however, produces some non-uniformity along the feed direction. Usually, stress components are averaged on several equi-spaced vertical lines distributed in one single feed pitch.
- Numerical residual stress predictions are sometimes coherent with the measures just in terms of parametric trends, though significant differences can arise. Unfortunately, these large divergences usually are at the surface, where the assessment of the residual stresses are of major importance e.g. for fatigue.

An experimental parametric investigation on aluminium alloy 7075-T6 is reported in this paper by showing in depth residual stress distributions for increasingly load and different feed values, generated with this conical and rounded roller shape. A comparison analysis and related discussion is provided in terms of parameter sensitivity on residual stress distributions. FE simulations, with a plain strain model, are also reported in order to have an assessment of the work hardening, for each investigated combinations of load and feed, to be evaluated along with the residual stress trends.

2. Experimental setup

2.1. Aluminium alloy 7075-T6 mechanical characterization

As mentioned in the Introduction, the deep rolling specimens were extracted from aluminium alloy 7075-T6 bars. Tensile tests, reported in Fig. 1, confirmed literature data for this material: Young's modulus $E = 71\,500$ MPa, Yield and Ultimate strengths: $S_Y = 540$ MPa, $S_U = 580$ MPa respectively. Being S_U such not largely higher than S_Y, the hardening of the material is small. A clear consequence of this very limited work hardening is that the initial yield strength limits the maximum residual stress any mechanical treatment can induce, as experimentally found and discussed in this research. During deep rolling, the surface material experiences multiple loadings after initial hardening. For this reason, a further non standard test was performed to find the stress-strain cyclic behaviour of this material, Fig. 1 (b). After a tensile stress of 580 MPa, the imposed deformation rate was reversed, and the compressive yield was then experienced at a smaller stress: (minus) 490 MPa, thus showing the Bauschinger effect. Moreover, the cyclic curve showed a smoother transition from elastic to elasto-plastic, at the yield point, rather than the monotonic curve. This specific material behaviour was then modeled in the FE simulations reported below.

2.2. Deep rolling tool

The DR operations were performed with a tungsten carbide roller tool: model D90-L-25-0 by DREX-TOOLS, very similar to that shown and used by Tian and Shin for laser-assisted burnishing [40]. As mentioned in the Introduction, the geometry of this tool is conical with a rounded fillet at the contacting edge. This device can be used with a common machine tool, such as milling or turning machines. The tungsten carbide indenter is supported by needle bearings, thus pressurized fluid is not required, moreover, the process can even be performed just as dry contact, though lubrication with the machining coolant fluid is recommended. The geometry and the positioning of the roller tool is reported in Fig. 2 (a). The nominal edge radius, as reported by the manufacturer is $r_R = 0.78$ mm. After verification of the geometry, with a profilometer, the value of the actual radius was found $r_R = 0.744$ mm, so very similar to the nominal. The clearance angle was not given by the manufacturer.

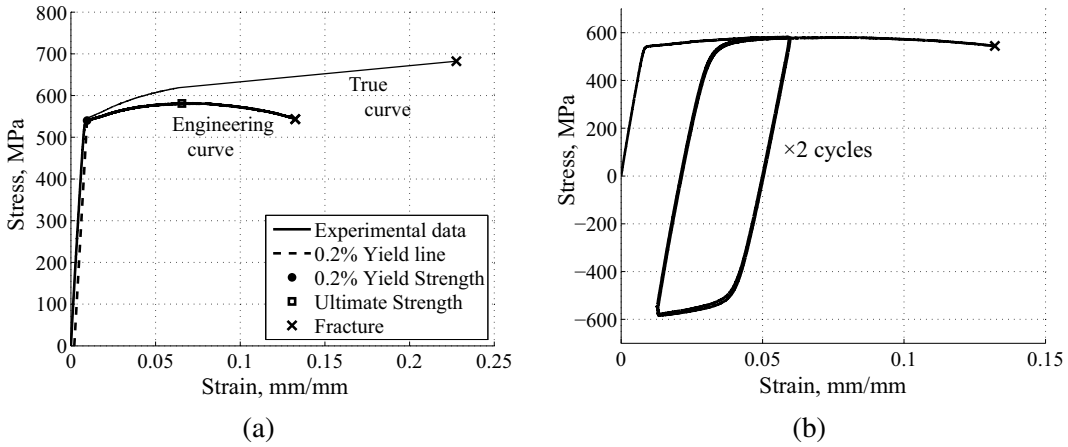

Figure 1: (a) Tensile test on 7075-T6, engineering and true curve. (b) Cyclic curve after initial work hardening.

A measure of this value was obtained by evaluating the profile of an indentation region and it was found approximately $\alpha = 1.6°$. Fig. 2 (b) shows the roller trace, after an initial vertical indentation. The front and rear regions of radius and cone surfaces are evident, the rolling motion can have either left or right direction, while the recommended feed orientation is from the cone to the radius. Material pile-up is also evident in Fig. 2 (b). The subsequent edge contacts produce surface unevenness mitigation and pile-up shifts (each shift is obviously equal to the feed length) leaving the treated back surface significantly smoother then the previous machining.

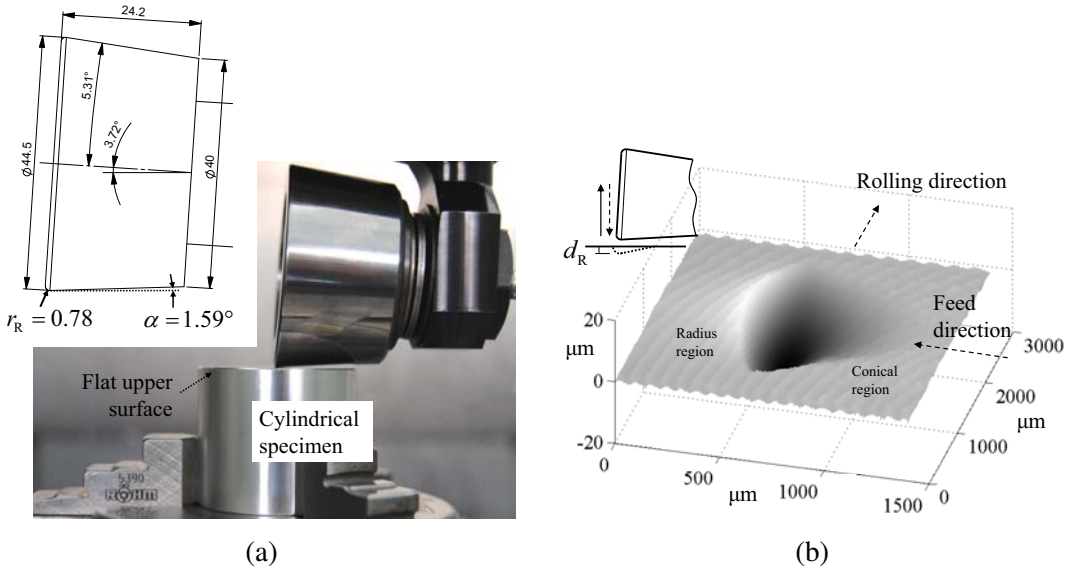

Figure 2: (a) Deep rolling tool and geometry dimensions of the carbide roller. (b) Roller trace after initial vertical indentation (non proportional scales).

2.3. Deep rolling normal force

The vertical load with this kind of rolling tool was induced by a normal displacement δ_N, after initial contact, just imposed to the milling (or turning) machine as a depth of cut. The tool support can freely move inside its track and the toolholder internal surface is lubricated in order to reduce friction. A small stiffness, from the roller contact to the toolholder, is recommended in order to have a reliable control of the vertical load. A stack of disc springs is inserted between the two parts of the support, finally, the upper point of the support is in contact with a load cell to accurately measure the load during the rolling, Fig. 3. A similar tool setup, with spring and load cell, was proposed by Shiou and Chuang [41] along with a ball type roller. However, the low plasticity burnishing

sphere is usually supported by the pressurized fluid to ease the rolling, while the indenter used here is supported by needle bearings and this solution can not be replicated for the spherical tool.

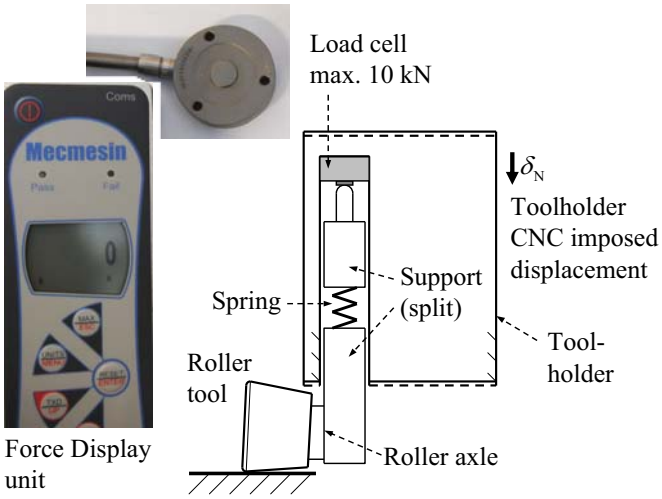

Figure 3: Scheme of normal force measurement during rolling.

The normal force was just "open loop" controlled. The force was only read during the rolling operation, instead of feedback controlled. However, the numerical control accuracy, the fine surface preparation of the specimens, and the low stiffness of the inserted disc springs allowed to have a good stability of the rolling force F_N after a preliminarily setting of the normal displacement δ_N. Fig. 4 shows the relation between δ_N and the measured normal force F_N for single point indentations, as shown in Fig. 2 (b). On the same graph it is also reported the depth of residual indentation d_R, after tool removal, that was measured by means of a contact profilometer. Though much smaller, this depth had a very similar trend with respect to the normal displacement δ_N that is mainly due to the low stiffness of the springs and specimen elasticity rather than plasticity yielding. After setting the vertical indentation, the normal force did not change significantly during subsequent rolling. The force fluctuation was approximately in the range ± 10 N, as shown below. Though not reported in this work, the normal force was observed to be more stable during rolling on a turning machine, being the rolling process not discontinuous, rather than on a milling machine. As a consequence an even smoother final surface was obtained on turning.

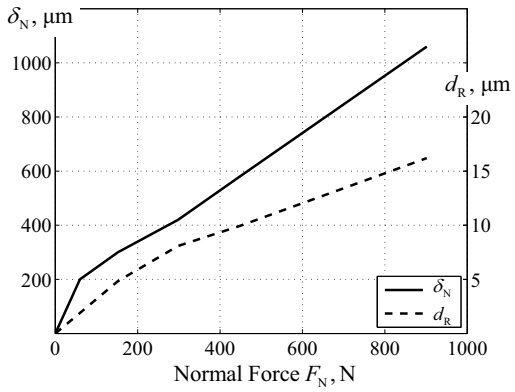

Figure 4: Vertical displacement and residual indentation depth dependencies with respect to the normal force, obtained with single vertical indentations.

2.4. Deep rolling feed

The deep rolling tests reported in the present paper were obtained on the flat surface of small cylinders to be then investigated with residual stress measurement techniques. A milling machine (HAAS Super Mini Mill) was used to generate an array of rolling traces. The feed f is the distance between rolling subsequent traces. Fig. 5 (a) shows the tool path along with the feed definition. The imposed feed was very accurately reproduced by the numerical control machine. Observations of the rolling traces confirmed an error on the feed not larger than 1%, Fig. 5 (b).

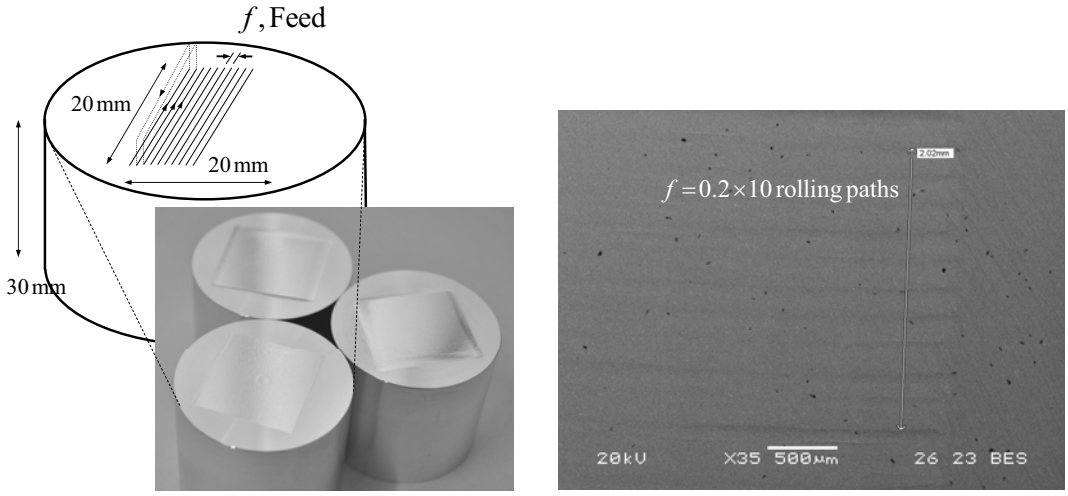

(a) (b)

Figure 5: (a) Imposed deep rolling path and feed definition. (b) Verification of the feed by SEM observation of a rolled surface.

2.5. Tested parameter combinations

As mentioned in the Introduction, the DR process parameters are rolling speed, number of passes, feed and rolling force. The deep rolling tests reported here were just performed with a small rolling speed to avoid tool chattering, and also to avoid specimen surface temperature rise, indeed the rolling process was performed under dry condition without machining coolant. Moreover, the performed rolling was just single pass, future work can reveal any improvement of multiple passes but overhardening could be a drawback, as discussed above. Hence, the parameters investigated in this research are the feed f and the normal force F_{N}. Test definitions and parameter combinations f, F_{N} are reported in Tab. 1.

	f, mm		
F_{N}, N	0.05	0.1	0.2
50	Test 1	Test 2	
150		Test 3	Test 4
300		Test 5	Test 6
450		Test 7	Test 8
900			Test 9

Table 1: Investigated parameter combinations and definition of the tests.

The initial contact was easily found as the force display onset, then the empirical relationship shown in Fig. 4 was used for setting the vertical displacement to be imposed as depth of cut to the numerical control. During rolling, the normal force experienced some fluctuations, both from the initial point to the final for any single rolling path, and from initial paths to end paths. As an example, these force variations are reported in Tab. 2 about Test 3 for which the nominal force was $F_{\mathrm{N}} = 150$ N. Measured force values at different rolling positions

were also statistically evaluated as mean and standard deviation. Force values recording and statistical analyses were performed for all the tests, mean and standard deviation results are reported in Tab. 3.

Initial rolling paths		Final rolling paths	
begin point	end point	begin point	end point
164	168	146	150
160	162	148	152
160	162	150	154
Average value $F_{N,av} = 156$ N			
Standard deviation $F_{N,std} = 7.2$ N			

Table 2: Measured normal force values F_N (in Newton) at different rolling positions for Test 3.

	F_N, N (nominal)	F_N, N (average)	F_N, N (st. dev.)
Test 1	50	57	13.7
Test 2	50	69	3.0
Test 3	150	156	7.2
Test 4	150	145	4.3
Test 5	300	308	11.3
Test 6	300	306	4.4
Test 7	450	457	5.7
Test 8	450	460	2.4
Test 9	900	933	5.9

Table 3: Normal force statistical values for all deep rolling tests.

3. Deep rolling surface modification

3.1. Surface roughness

Deep rolled surfaces were investigated with a contact profilometer. Fig. 6 (a) shows the Test 9 tree-dimensional relieved initial and final portions of the deep rolled surface. The front region of the rolled surface clearly shows a rising wake ahead of the tool due to the material pile-up. The height of this wake depends on the rolling force and it ranged from a few microns for the lowest investigated rolling load values, to a few tens of microns for the highest rolling loads. This plastic wake has not a detrimental effect on the surface roughness since it is flattened after each subsequent passage, as shown in the FE simulation section reported below. Fig. 6 (b) reports single profiles for roughness evaluation, both just after turning and then after deep rolling. R_a reduction more than a factor of 2 is evident. Test 3, with a much smaller force and also smaller feed, reported very similar roughness values: $R_a = 0.69$ µm after turning, $R_a = 0.25$ µm after deep rolling. A preliminarily test with $F_N = 450$ N, $f = 0.2$ mm was performed with a much coarser turning surface, and after rolling the surface roughness was again improved approximately by the same factor: $R_a = 1.38$ µm after turning, $R_a = 0.54$ µm after deep rolling. Though not intensively investigated in this paper, apparently, the average roughness is primarily related to the surface finish before deep rolling and less affected by the rolling parameters force and feed. This is basically in agreement with the literature, such as the paper by Rodríguez et al. about ball-burnishing [7]. Finally, the surface roughness values obtained with this conical and rounded tool are well inside the typical range of grinding roughness, so for some applications deep rolling could replace grinding itself.

3.2. Surface hardness

The surface hardness was also measured on the deep rolling specimens. The reference 7075-T6 hardness value was 175 HV without deep rolling or any other mechanical surface treatment. This result was experimentally

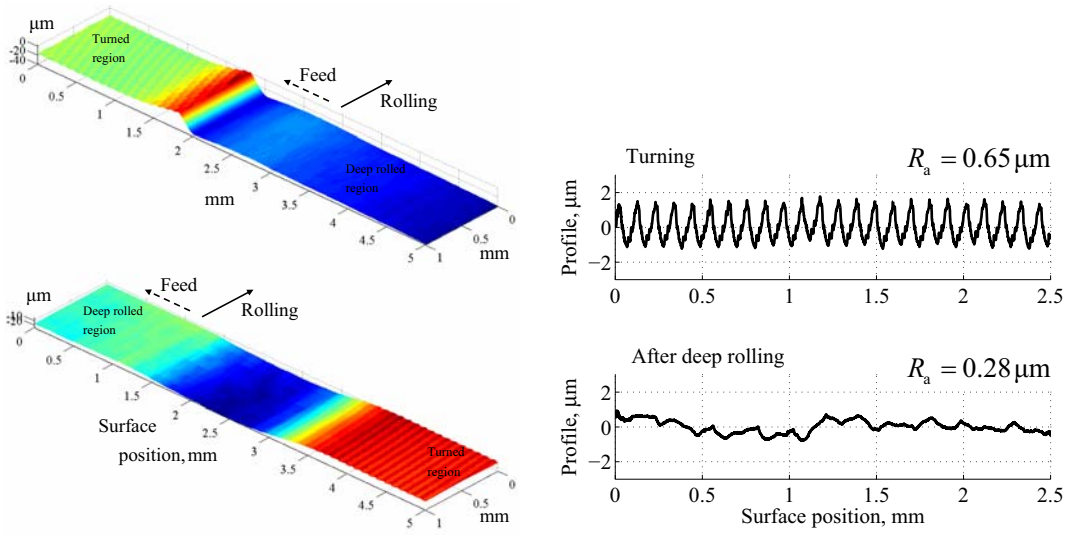

Figure 6: (a) Relieved surface at the treatment extremities. (b) Roughness reduction after deep rolling.

found in the present research and was in agreement with the literature data, e.g. Ref. [12]. Though the limited work hardening, as evident from the tensile tests, Fig. 1, the hardness slightly increased because of deep rolling. Parametric results are reported in Tab. 4. Both feed and rolling force influenced the surface hardness. Higher rolling force produced an increase of hardness, as well as closer rolling passes (smaller feed) positively contributed to the hardness. Among the two parameters, feed has a predominant effect. E.g. in the range of rolling force $150-450$ N the hardness was steadily 188 HV5 with $f = 0.1$ mm, while the feed still produced an effect of $2-5$ hardness points. Very strong combinations of feed and load were finally tested to have a highest reference value. The maximum obtained hardness was 196 HV5, that was in good agreement with maximum (micro-)hardness reported by Benedetti et al. [12] about the strongest shot peening on the same alloy and similar heat treatment.

No deep rolling: 175			
	f, mm		
F_N, N	0.05	0.1	0.2
50	186	179	
150		188	182
300		188	186
450		188	183
900			186
1000	196	193	

Table 4: Hardness HV with 5 kgf load, parametric comparison on deep rolled specimens.

4. Deep rolling residual stresses

4.1. Residual stress measurement techniques

Common techniques for experimental measurement of residual stress distributions induced by surface treatments are the X-Ray Diffraction (XRD) and the Hole Drilling Method (HDM). The theory of the XRD technique is available in several books and papers such as the handbook by Lu [42], the standard BS EN 15305:2008 [43] and the papers by Prevéy [44, 45]. In this research the system Xstress 3000 G2 (by Stresstech) was used. This

diffractometer is based on the Bragg's law and it is specifically designed for the residual stresses. According to Refs. [44, 45] about measurements on aluminium alloys, the Chromium source (radiation Cr Kα) was used with a diffraction angle $2\theta = 139°$ and crystallographic plane (311) for the lattice spacing derivation. The $\sin^2\psi$ method was performed with a ψ range from $-40°$ to $+40°$ divided in 9 tilt positions and oscillations of $\pm 3°$ each tilt. The collimator diameters size was 3 mm, and the X-ray penetration depth was approximately $10-12$ µm. The hole drilling method is based on material removal and relaxed strain gauge readings. A stepped hole is introduced concentric with a rosette gauge and the residual stress distribution is obtained after relaxed strain elaboration. The automatic system RESTAN–MTS3000 (by SINT Technology) was used here and the analytical algorithm for residual stresses back-calculation from the relaxed strain measurements was introduced and developed by Beghini et al. [46, 47, 48, 49]. Hole drilling accuracy assessment was provided by Grant et al. [50], and direct validation of HDM was performed by Valentini et al. [51, 52] with a dedicated bending test rig. Successful comparison between XRD and HDM were also published by Grant [53], Fontanari et al. [54], and more recently by Valentini et al. [23].
Both residual stress measurement techniques were used in the present paper by exploiting the peculiarities of the two different methods [23, 55]. The HDM allowed to measure the residual stress distributions up to 1 mm in depth, and the XRD was then used for validation at the surface and at the very initial subsurface. A hole drilled strain gauge rosette, applied on a deep rolled specimen, is shown in Fig. 7 along with the definitions of feed and rolling directions and consistent residual stress components.

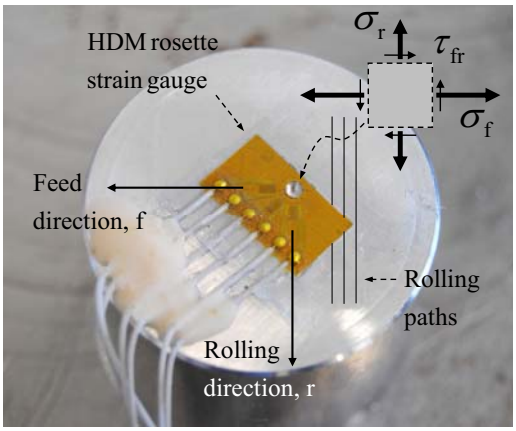

Figure 7: Hole drilling method, strain gauge rosette and definition of the residual stress components.

4.2. Residual stress distributions

Preliminarily tests were performed on specimens without any rolling, just after a fine turning finish. The residual stresses, measured with HDM, were found to be quite low and tensile at subsurface. The XRD testing reported a low compressive value at the surface, on a different specimen, prepared with the same turning finish. These two measurements are reported in Fig. 8, the residual stress components are here just termed as $\sigma_x, \sigma_y, \tau_{xy}$ being feed and rolling directions not yet introduced. After the evidence of these small values, the residual stresses induced by the turning finish, before rolling, were simply assumed as negligible and the residual stress (shown below) were completely attributed to the deep rolling operation.
Residual stress measurements were performed on all the rolled specimens whose parameters are listed in Tab. 1. HDM measurements were applied at two points apart (each specimen) inside the rolled area and not close to the boundaries. Then XRD measurements were also performed on intermediate points of each specimen previously HDM tested. Some specimens were tested even with two XRD measurements, while just one for others. Furthermore, some of the single XRD measurements were repeated on different specimens (with the same rolling parameters) just for validation, obtaining very similar results. Fig. 9 shows HDM and XRD measurements on two tests. The stress components are here referred to σ_f feed direction, σ_r rolling direction and τ_{fr} shear, according to the scheme of Fig. 7. Not large differences were found between the two point measurements and between

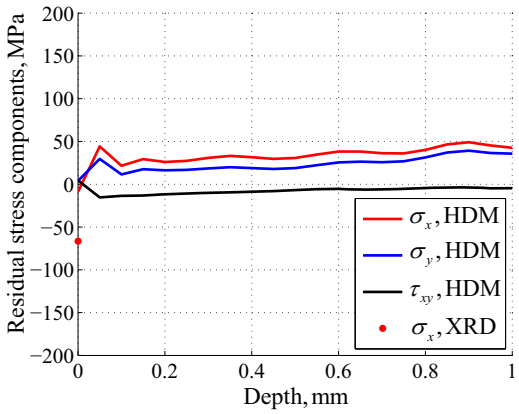

Figure 8: Residual stress after turning and no deep rolling.

the two techniques. Discrepancies were mainly evident at the surface, though between the typical uncertainty ranges. Moreover, some non-uniformity of the deep rolling treatment, at different positions of each specimen, should also be considered. Since the maximum depth of the XRD measurements was quite small (it never exceed 0.1 mm) and the specimens had high stiffness, at least not bending compliance, the material removal effect on residual stresses was negligible [44]. For this reason, no correction was applied to the in-depth values obtained after electropolishing material removal and subsequent XRD measurement on the newly exposed surface.

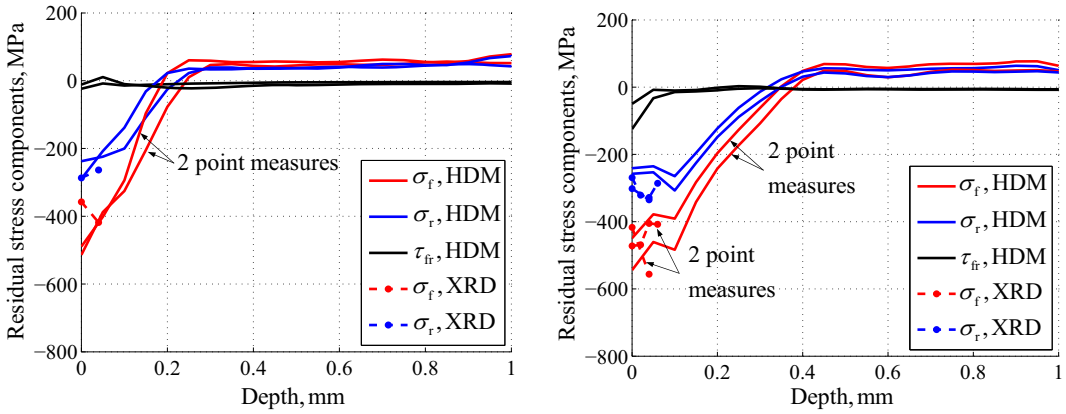

Figure 9: Residual stress measured with HDM and XRD, for different parameter combinations: (a) Test 2, $F_N = 50$ N, $f = 0.1$ mm; (b) Test 3, $F_N = 150$ N, $f = 0.1$ mm.

The shear stresses τ_{fr} were very small for all the investigated specimens, Fig. 9. After having found zero (or negligible) shear stress along the entire measurement depth, no stress rotation was required and the feed and rolling obviously were just the principal directions. The shape of the roller itself and the deep rolling process was also suggesting these principal directions. Now this intuitive assumption is experimentally validated and, hereafter, σ_f and σ_r are regarded as the principal residual stresses and reported without the shear component. Average values were calculated by taking into account both HDM and XRD measures at surface and at initial subsurface depths, while only HDM values were averaged for further depths. After this multiple measurement and averaging procedure, a unique distribution of σ_f, σ_r (principal) components was associated to each deep rolling test. A remarkable evidence about all test distributions is that the two residual stress components are quite different. The feed is larger than the rolling component, approximately by a factor of 2 at the surface and at the subsurface, while the two components are almost equal, and quite low, after sign reversal. As mentioned in the Introduction, the reason of this anisotropy is both the high curvature ratio, at the contact region, and the preferential feed direction of the plastic deformation process.

4.3. Parametric analysis

Two feed values were tested for the investigated normal forces: $50, 150, 300, 450$ N. Fig. 10 shows the effect of the feed for each single force value. It is evident that a factor of 2 on feed produced small effects below the surface, that can even be confused with the measurement accuracy or treatment non-uniformity. E.g. subsurface residual stress components were higher for larger feed in Fig. 10 (a) ($F_N = 50$ N), while they were smaller in Fig. 10 (b) ($F_N = 150$ N). Nevertheless, the feed produced a detectable effect on the stress gradient in the initial subsurface depth range: $0.0 - 0.1$ mm. The compressive surface residual stresses were higher (absolute values) for the smaller feed, especially for the lower normal forces, Fig. 10 (a), (b) and (c), while for higher normal force the effect is more pronounced on the subsurface residual stress maxima, Fig. 10 (d).

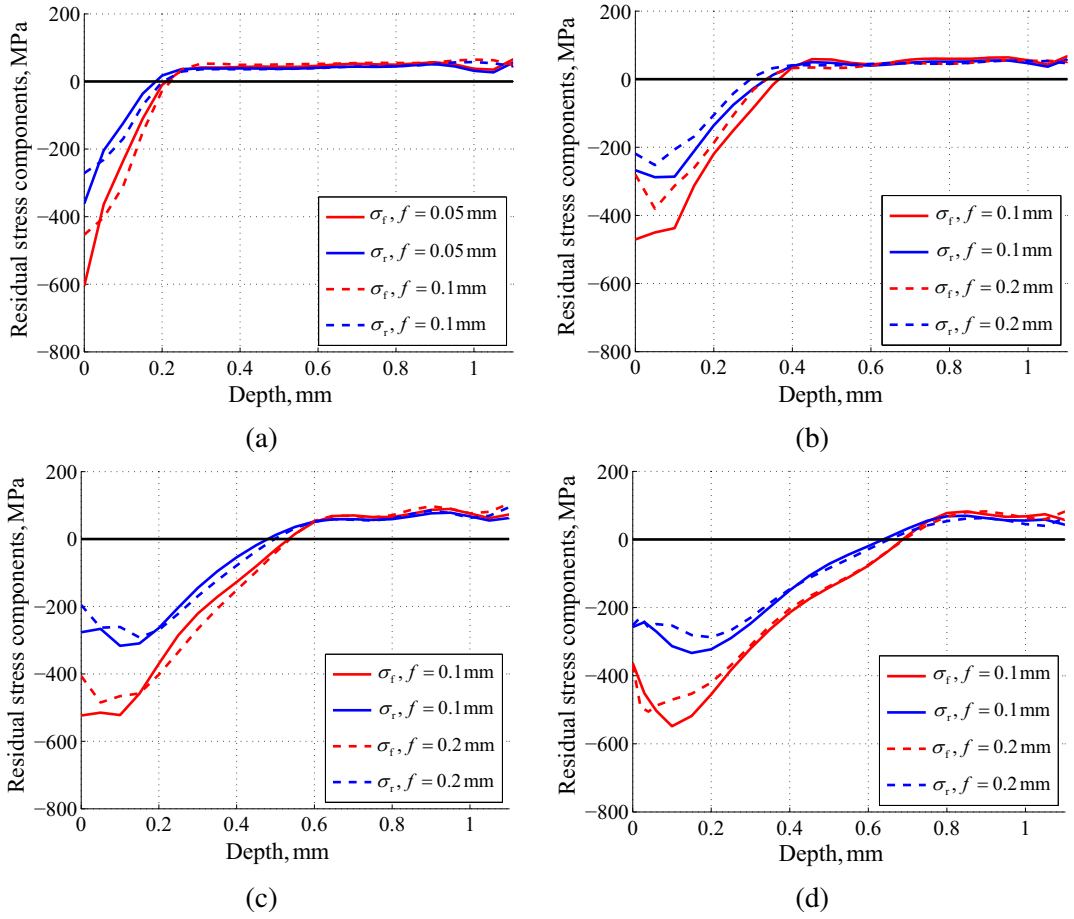

Figure 10: Feed sensitivity on residual stresses: (a) $F_N = 50$ N, (b) $F_N = 150$ N, (c) $F_N = 300$ N, (d) $F_N = 450$ N.

On the contrary, the rolling force produced a remarkable effect on the overall residual stress profiles. Fig. 11 shows the comparisons with same feed values and increasingly rolling normal forces. A parameter clearly driven by the rolling force is the depth of compressive residual stress d_c. This depth is here defined as the average of the compressive to tensile transition depths for the two residual stress components, being these two depths very similar for each distribution. d_c increased with F_N, without being significantly affected by the previously investigated feed parameter f, that is just effective at the surface and the very initial subsurface, as previously pointed out.

4.4. Depths of compressive and maximum residual stresses

The relation between the depth of compressive residual stress and the rolling force is reported in Fig. 12. The depths of the maximum residual stress components, rolling and feed $d_{r,max}, d_{f,max}$ are also shown in the same figure. Increasing trends are evident: the higher the rolling force the deeper the compressive depth, as mentioned

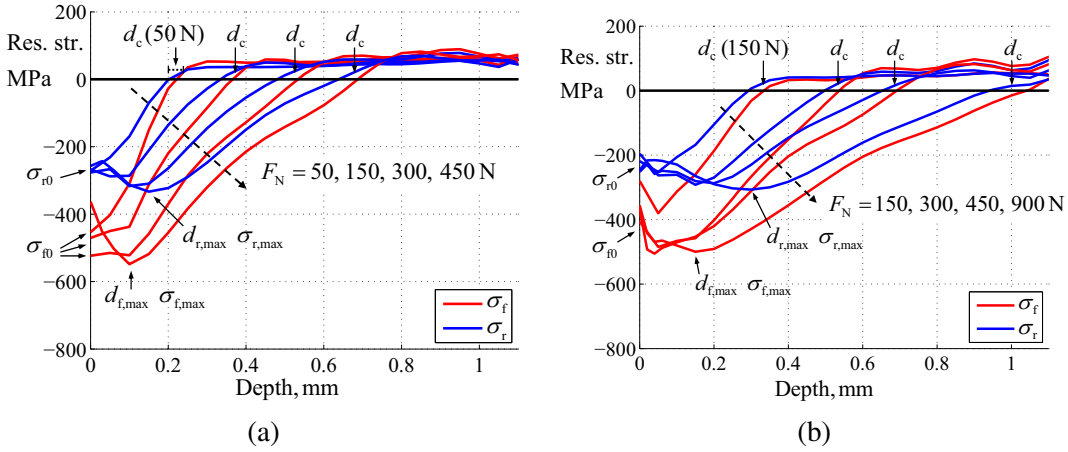

Figure 11: Rolling force sensitivity on residual stresses: (a) $f = 0.1$ mm, (b) $f = 0.2$ mm.

above, and the deeper the residual stress maxima too. About these latter depths, also the feed has a role. As a general trend, the lower the feed the lower the depths of maximum stress. More specifically, the feed stress component just keeps its maximum at the surface up to the normal force value $F_N = 300$ N for the feed value $f = 0.1$ mm, while it is subsurface for $f = 0.2$ mm.

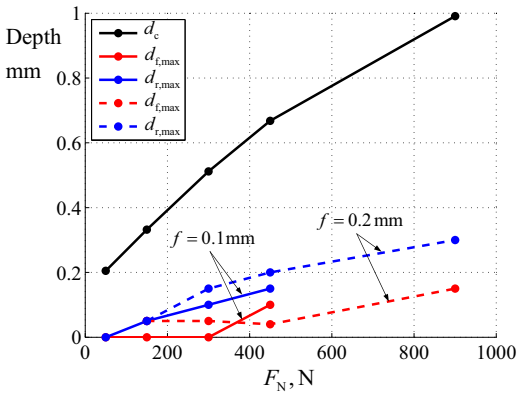

Figure 12: Trends of compressive depth and subsurface maximum residual stress depths.

Finally, the surface and the maximum residual stresses are reported in Fig. 13 (a) and (b) respectively, for the two feed values: $f = 0.1 - 0.2$ mm. Both surface and maximum subsurface stress components were higher for the lower feed. Nevertheless, there was not an evident trend for the surface values with the force, while the subsurface maxima kept a slight increasingly trend.

The yield stress limit is quite evident here. Though largely different tested parameters, the feed maxima were always very close to the yield stress $S_Y = 540$ MPa, Fig. 13 (b). As mentioned above, the material small hardening behaviour did not allow a significant increase of the yield stress during the plastic deformation process. While the maximum stress remained quite similar to the yield stress, the position of the maximum shifted at subsurface by increasing the rolling force, as shown previously. Being the maximum limited, and located below the surface, necessarily the residual stresses at the surface reduced. This trend needs to be carefully considered in order to evaluate the optimum selection of the process parameters. E.g. for fatigue strength enhancement, a large compressive depths is obviously attractive, but a smaller surface compressive stress may be detrimental, or at least not optimal, being the fatigue crack initiation at the surface. A complete overview of the residual stress distributions obtained with experimental measurements, as provided here, is therefore a very useful reference for effective treatment parameter selection.

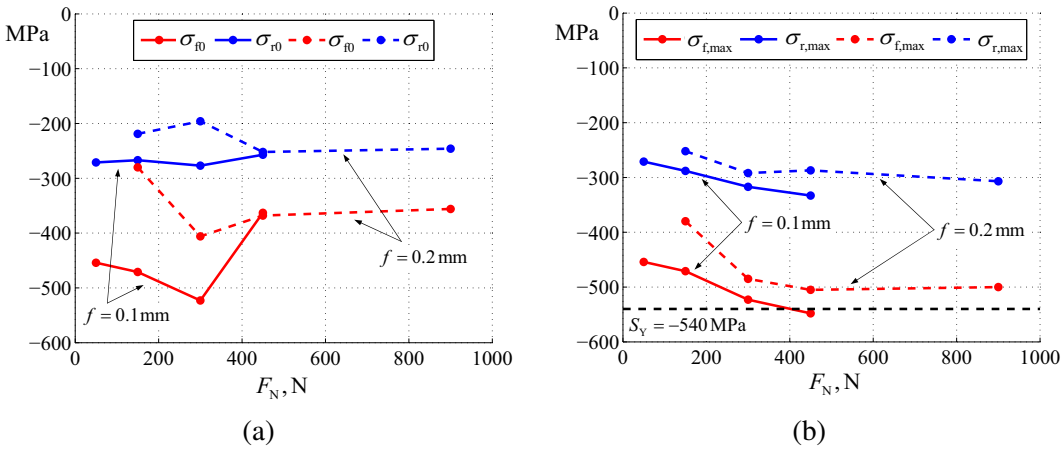

Figure 13: Feed and rolling residual stresses: (a) at the surface and (b) maximum.

5. FE analysis

5.1. Model setup

As discussed in the Introduction, FE analyses of rolling process is a challenging task. One of the main limitations is the plane model, instead of a fully 3D, to have accurate mesh discretization especially at the surface and at the initial subsurface depths, and also to have far boundary conditions. The rolling tool investigated in the present study shows a high curvature edge aligned with the feed direction, while the curvature is much smaller along the rolling direction. For this reason, the model was implemented as plane strain, with the plane perpendicular to the rolling direction. The indentation process was, therefore, simulated as vertical penetration of the tool section profile. The indentation was repeated several times at subsequent steps whose spacing was obviously equal to the feed, Fig. 14 (a). Plane strain 4-node elements were used along with surface-to-surface contact and target. A gradient mesh was prepared in order to have very accurate discretization in the initial subsurface depth were the residual stress and plastic strain results are evaluated. The minimum element size was 2.5 µm, this size was suggested by a preliminarily convergence analysis on a benchmark Hertz model. The total number of elements (structural solid and contact) was approximately 115 000. The lower boundary was placed at a remarkable distance with respect to the indentation region, not reported in the figure, and the far lateral boundaries allowed a large number of subsequent indentations: approximately 50 for $f = 0.1$ mm. This wide simulated indentation region was required to have a reliable stabilization of the residual stresses. The indentation tool was modeled just as a rigid profile being the tungsten carbide roller much stiffer than the aluminium alloy specimen. Frictionless contact between the rigid indenter and the specimen was introduced. Multilinear kinematic hardening material model was implemented, for the aluminium alloy, according to the Bauschinger effect observed before and reproducing the monoxial cyclic curve, Fig. 1 (b). The simulation results were finally extracted at the mid position of the multiple indentation width to have very limited residual stress perturbation due to the lateral boundaries. The residual stresses were evaluated after the final indentation, with the indenter profile at upper position, hence not in contact with the simulated specimen. The residual stress were post-processed by averaging the results on a large number of multiple paths equally spaced inside a feed length, Fig. 14 (b), in order to have uniform values along the feed direction. Convergence analysis allowed to select an adequate number of paths equal to 20 (in the figure a smaller number is reported just for graphical clarity).

The pressure evolution during the simulated rolling process is reported in Fig. 15 that shows the contact distribution at different steps while the roller is driven to its lowest position. Initially, a slightly perturbed Hertzian distribution arises, then it is evident that the maximum pressure is limited by the yield of the material while the plastic wake is flattened (as well as any surface roughness, though not modeled here) and the contact widens toward a portion of the previously treated region.

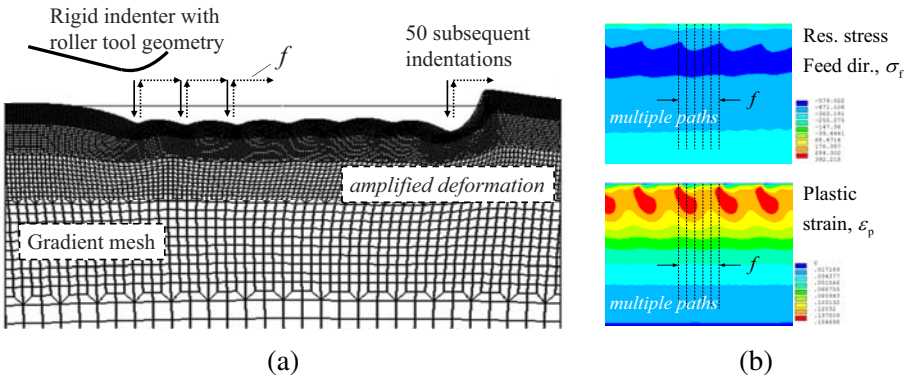

Figure 14: (a) FE model, mesh and indentation path of the roller tool profile. (b) Residual stress and cumulative plastic strain, multiple calculation paths for averaging.

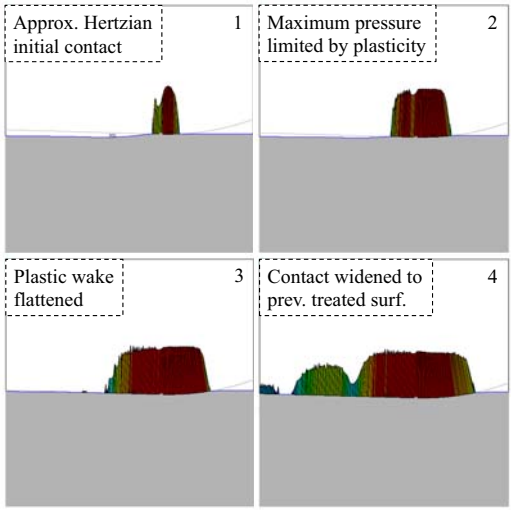

Figure 15: Contact pressure evolution during the flattening of the plastic wake.

5.2. Accumulated plastic strain

The depth of imposed indentation in FE simulations was tuned in order to have an accurate prediction of the subsurface residual stress distributions. As an example, Fig. 16 shows the comparison between experimental and FE stresses for Test 7 along with the resulting simulated plastic strain. The stresses at the surface and at the initial subsurface were not perfectly matching the experimental data. The numerical analyses predicted very strong stress gradients at the surface, that could not be captured by the measuring techniques, moreover, the prevented material flow along the out-of-plane direction, as modeled with plane strain, is more incisive at the initial subsurface where the plastic strain is higher.

Nevertheless, this kind of simulation was still considered a valid estimator of the accumulated plastic strain during the deep rolling process, otherwise not directly related to the measured residual stresses. As shown in Fig. 16, the aforementioned compressive depth was very similar to the maximum depth where the material experienced plastic strain. Similarly to the compressive thickness, this plasticity depth was only dependent on the rolling force (or alternatively a stress parameter such as the elastic Hertzian pressure) with a very limited contribution of the feed, Fig. 17 (a). Nevertheless, the maximum of the plastic strain distribution $\varepsilon_{p,max}$ was found to be dependent on the normal force and the feed too, Fig. 17 (b).

Despite the limited effect of the feed on residual stresses, the entire distribution of plastic strain (and so the maximum) was increased by almost a factor of 2, that merely coincides with the ratio of the feed values, for all the investigated rolling forces. After this numerical analysis it is evident that small feed can generate excessive hardening with a small beneficial contribution on the residual stresses, that are just limited by the yield. This

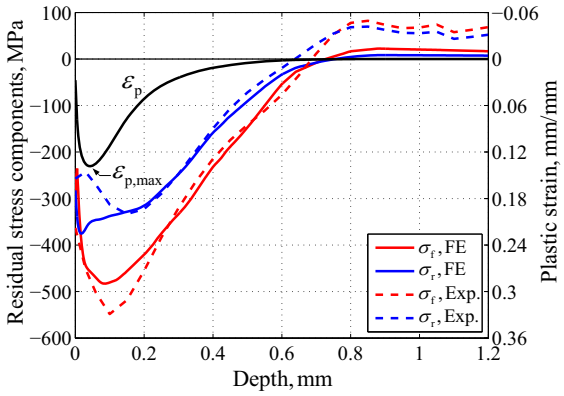

Figure 16: Comparison between experimental and FE residual stresses, and simulated plastic strain distribution.

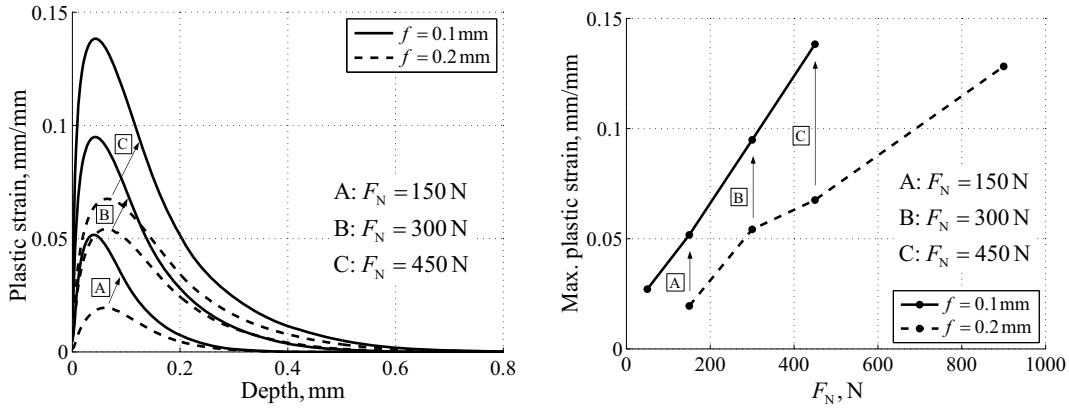

Figure 17: (a) Accumulated plastic strain distributions produced by different force and feed combinations. (b) Plastic strain maxima depending on load and feed.

high work hardening is not attractive since it implies embrittlement, thus very small feed should be avoided, anyway a definite allowable maximum plastic strain need to be assessed for any specific material and in-service loading.

6. Discussion

Some trends of the obtained distributions are finally compared here to the literature results and discussed. An evident result found in this investigation is that the plasticity depth is overlapping the residual stress compressive depth. This result is in agreement with the paper by Bijak–Żochowski and Marek [56] for large size rolling and also with the paper by Valentini et al. [51] where the shot peening compressive depth was almost equal to the maximum depth of the micro-hardness profile, that in turn is related to the material plasticity. Furthermore, the plasticity percentage reported by Prevéy and Cammett [16], same aluminium alloy 7075-T6, was approximately 20% for the low plasticity burnishing (while it was 40% at the surface for the shot peening) and this is quite in agreement with the maximum accumulated plasticity reported above that never exceed 15%. Even the highest compressive residual stress is coherent with the present paper result, being just slightly larger than the (initial) yield stress of the aluminium alloy.

Many investigators usually report the in-depth comparison between shot peening and deep rolling, such as Prevéy and Zhuang and coauthors [16, 19, 20, 57], just to show how the former treatment is significantly shallower than the latter. The typical depth of the shot peening is a few tenths of a millimeter [12, 31, 57], mainly depending on the shot size and on intensity too, while the low plasticity burnishing, as well as the present deep rolling results,

have a size depth up to 1 mm. The shot peening process obviously is isotropic since it has not a preferential direction [23]. For this reason, the obtained residual stress is equi-biaxial, in fact just a single stress component is usually plotted versus the depth. The low plasticity burnishing is sometimes also reported just with a single component albeit the equi-biaxial property is questionable. Though the spherical tool, low plasticity burnishing is not isotropic because the treatment has again two specific directions: rolling and feed. While the papers by Klocke et al. reported almost equi-biaxial roller burnishing residual stresses [14, 38], the papers by Rodríguez et al. [7], Avilés et al. [58] and Sartkulvanich et al. [34] showed very different stress components along these two directions. More specifically the feed (or axial) direction stress is approximately a factor of 2 with respect to the other component, basically the same as obtained here with the conical and rounded roller. Similarly, the papers by Tian and Shin [40], Balland et al. [29] and also Majzoobi et al. [59], reporting residual stress results about roller with two different curvatures, again, showed a stress component ratio approximately of 2. Apparently, the plasticity process has a predominant role, at least on the principal residual stresses, with respect to the curvature ratio, thus reducing the significance of the roller shape.

7. Conclusions

Deep rolling with a conical and rounded tool was investigated in this paper in terms of roughness, hardness, induced residual stresses (experimental) and accumulated plasticity (FE simulation) on a high strength aluminium alloy. The surface roughness was found more significantly affected by the initial surface preparation, due to the previous machining, rather than the rolling parameters. Approximately a reduction factor of 2 was observed, that allowed to obtain roughness values typical of the grinding operation. Both rolling force and feed had an effect on the surface hardness. High load and small feed contributed to higher hardness and the obtained maximum value was 196 HV starting from the untreated surface 175 HV. Residual stresses were measured with combined X-ray diffraction and hole drilling methods. A parametric analysis was proposed with different combinations of rolling force and feed. The main results of this comparative study are summarized in the following:

- The principal residual stresses were aligned with the rolling and the feed directions.
- The investigated conical and rounded tool introduced quite large different residual stresses along the two principal directions. Similarly to the ball type burnishing, the feed direction residual stress at the surface was approximately a factor of two higher than the other component.
- The feed parameter mainly influenced the very initial subsurface stress gradient. The surface compressive residual stresses were slightly higher (absolute value) with a smaller feed. On the contrary, the deeper residual stress distribution was very marginally influenced by the feed.
- The rolling force had a significant effect on the entire stress distribution, hence the depth of compressive residual stress was primarily related to the force with negligible effect by the feed.
- The positions of the maximum stress, for each component, was also investigated and related to the parameters. Smaller feed tended to keep the maxima at the surface, while higher normal load drove the maxima below the surface.
- The maximum stress was very clearly limited by the material yield stress, especially being the investigated aluminium alloy low hardening. As a consequence, high rolling force produced a shift of the maximum depth, but merely not an increase of the maximum itself, thus the residual stresses at the surface tended to reduce.
- Finally, the FE model showed that the plastic strain distribution was primarily affected by the normal force in terms of depth while the maximum level was remarkably influenced also by the feed, though the limited effect on the surface and the initial subsurface residual stresses, as discussed before.

This overview of residual stress distributions and the sensitivity to deep rolling parameters is very useful to optimize the treatment for a specific target, such as for fatigue strength enhancement. A very small feed is to be avoided since it produces severe work hardening with a limited effect on surface and subsurface residual stresses that are just limited by the yield stress. Even a strong rolling force is not advisable. Very large compressive depth is unnecessary when the fatigue process volume is small (such as high strength alloys), in addition high hardening again results, and the maximum residual stress can shift at subsurface, hence not completely effective for preventing surface fatigue crack.

Acknowledgments

This work was carried out as part of the Italian research program PRIN 2009Z55NWC. The Authors would like to express their gratitude for the funding. Brusa Meccaniche company (Livorno, Italy) is also acknowledged for performing the deep rolling treatments. Finally, the authors are very grateful to Peen Service company (Bologna, Italy) for the X-ray diffraction measurements.

References

[1] K. Skalski, A. Morawski, and W. Przybylski. Analysis of contact elastic–plastic strains during the process of burnishing. *International Journal of Mechanical Sciences*, 37(5):461–472, 1995.

[2] M.H. El-Axir. Investigation into roller burnishing. *International Journal of Machine Tools and Manufacture*, 2000(11):1603–1617, 40. DOI: 10.1016/S0890-6955(00)00019-5.

[3] A.M. Hassan and A.S. Al-Bsharat. Influence of burnishing process on surface roughness, hardness, and microstructure of some non-ferrous metals. *Wear*, 199(1):1–8, 1996. DOI: 10.1016/0043-1648(95)06847-3.

[4] A.M. Hassan and A.M. Maqableh. The effects of initial burnishing parameters on non-ferrous components. *Journal of Materials Processing Technology*, 102(1–3):115–121, 2000. DOI: 10.1016/S0924-0136(00)00464-7.

[5] I. Altenberger. Deep Rolling: The Past the Present and the Future. In *9th International Conference on Shot Peening, ICSP9*, pages 144–155, 2005. Art. N. 2005065.

[6] P.R. Prabhu, S.M. Kulkarni, and S.S. Sharma. Influence of deep cold rolling and low plasticity burnishing on surface hardness and surface roughness of AISI 4140 steel. *World Academy of Science, Engineering and Technology*, 72:619–624, 2010.

[7] A. Rodríguez, L.N. López de Lacalle, A. Celaya, A. Lamikiz, and J. Albizuri. Surface improvement of shafts by the deep ball–burnishing technique. *Surface and Coatings Technology*, 206(11–12):2817–2824, 2012. DOI: 10.1016/j.surfcoat.2011.11.045.

[8] M. Guagliano and L. Vergani. Residual stresses induced by deep rolling in notched components. *Transactions on Engineering Sciences*, 8:109–119, 1995.

[9] G. Nicoletto and A. Saletti. Fatigue assessment of notched steel including residual stresses obtained by the rolling process. *SDHM Structural Durability and Health Monitoring*, 8(2):131–148, 2012.

[10] P.R. Prabhu, S.M. Kulkarni, and S.S. Sharma. An Experimental Investigation on the Effect of Deep Cold Rolling Parameters on Surface Roughness and Hardness of AISI 4140 Steel. *World Academy of Science, Engineering and Technology*, 60:1593–1598, 2011.

[11] P.R. Prabhu, S.M. Kulkarni, and S.S. Sharma. Experimental Investigations of Process Parameters Influence on Surface Roughness in Deep Cold Rolling of AISI 4140 Steel. *International Journal of Research in Engineering and Technology*, 1(3):159–163, 2012.

[12] M. Benedetti, V. Fontanari, P. Scardi, C.L.A. Ricardo, and M. Bandini. Reverse bending fatigue of shot peened 7075–T651 aluminium alloy: The role of residual stress relaxation. *International Journal of Fatigue*, 31(8–9):1225–1236, 2009. DOI: 10.1016/j.ijfatigue.2008.11.017.

[13] M. Benedetti, V. Fontanari, and M. Bandini. A simplified and fast method to predict plain and notch fatigue of shot peened high–strength aluminium alloys under reverse bending. *Surface and Coatings Technology*, 243:2–9, 2011. DOI: 10.1016/j.surfcoat.2011.12.008.

[14] F. Klocke and J. Liermann. Roller burnishing of hard turned surfaces. *International Journal of Machine Tools and Manufacture*, 38(5–6):419–423, 1998.

[15] L.N. López de Lacalle, A. Lamikiz, J. Muñoa, and J.A. Sánchez. Quality improvement of ball-end milled sculptured surfaces by ball burnishing. *International Journal of Machine Tools and Manufacture*, 45(15):1659–1668, 2005. DOI: 10.1016/j.ijmachtools.2005.03.007.

[16] P.S. Prevéy and J. Cammett. Low cost corrosion damage mitigation and improved fatigue performance of low plasticity burnished 7075-T6. *Journal of Materials Engineering Performance*, 10(5):548–555, 2001. DOI: 10.1361/105994901770344692.

[17] P.S. Prevéy and N. Jayaraman R. Ravindranath. Low Plasticity Burnishing (LPB) Treatment to Mitigate FOD and Corrosion Fatigue Damage in 17-4 PH Stainless Steel. In *Proceedings of the Tri–Service Corrosion Conference*, pages 1–11, 2003.

[18] P.S. Prevéy and J.T. Cammett. The influence of surface enhancement by low plasticity burnishing on the corrosion fatigue performance of AA7075-T6. *International Journal of Fatigue*, 26(9):975–982, 2004. DOI: 10.1016/j.ijfatigue.2004.01.010.

[19] P.S. Prevéy, N. Jayaraman, and J. Cammett. Overview of low plasticity burnishing for mitigation of fatigue damage mechanisms. In *Proceedings of ICSP 9*, 2005. Paper 260.

[20] W. Zhuang and B. Wicks. Mechanical Surface Treatment Technologies for Gas Turbine Engine Components. *Journal of Engineering for Gas Turbines and Power, ASME*, 125(4):1021–1025, 2003. DOI: 10.1115/1.1610011.

[21] S. Wang, Y. Li, M. Yao, and R. Wang. Compressive residual stress introduced by shot peening. *Journal of Materials Processing Technology*, 73(1–3):64–73, 1998.

[22] J. Schwarzer, V. Schulze, and O. Vöhringer. Evaluation of the influence of shot peening parameters on residual stress profiles using finite element simulation. *Materials Science Forum*, 426–432:3951–3956, 2003. DOI: 10.4028/www.scientific.net/MSF.426-432.3951.

[23] E. Valentini, C. Santus, and M. Bandini. Residual stress analysis of shot-peened aluminum alloy by fine increment hole–drilling and X–ray diffraction methods. *Procedia Engineering*, 10:3582–3587, 2011. DOI: 10.1016/j.proeng.2011.04.589.

[24] M. Benedetti, V. Fontanari, C. Santus, and M. Bandini. Notch fatigue behaviour of shot peened high-strength aluminium alloys: Experiments and predictions using a critical distance method. *International Journal of Fatigue*, 32(10):1600–1611, 2010. DOI: 10.1016/j.ijfatigue.2010.02.012.

[25] R.A. Cláudio, A. Burgess, C.M. Branco, and J. Byrne. Failure analysis of scratch damaged shot peened simulated components at high temperature. *Engineering Failure Analysis*, 16(4):1208–1220, 2009. DOI: 10.1016/j.engfailanal.2008.07.013.

[26] R.A. Cláudio, J.M. Silva, C.M. Branco, and J. Byrne. A fracture mechanics based approach to predict fatigue life of scratch damaged shot peened components. *Procedia Engineering*, 10:2672–2677, 2011. DOI: 10.1016/j.proeng.2011.04.445.

[27] C. Santus and D. Taylor. Physically short crack propagation in metals during high cycle fatigue. *International Journal of Fatigue*, 31(8–9):1356–1365, 2009. DOI: 10.1016/j.ijfatigue.2009.03.002.

[28] M.M. El-Khabeery and M.H. El-Axir. Experimental techniques for studying the effects of milling roller-burnishing parameters on surface integrity. *International Journal of Machine Tools and Manufacture*, 41(12):1705–1719, 2001. DOI: 10.1016/S0890-6955(01)00036-0.

[29] P. Balland, L. Tabourot, F. Degre, and V. Moreau. An investigation of the mechanics of roller burnishing through finite element simulation and experiments. *International Journal of Machine Tools and Manufacture*, 65:29–36, 2013. DOI: 10.1016/j.ijmachtools.2012.09.002.

[30] J. Mackerle. Coatings and surface modification technologies: A finite element bibliography (1995-2005). *Modelling and Simulation in Materials Science and Engineering*, 13(6):935–979, 2005. DOI: 10.1088/0965-0393/13/6/011.

[31] G.I. Mylonas and G. Labeas. Numerical modelling of shot peening process and corresponding products: Residual stress, surface roughness and cold work prediction. *Surface and Coatings Technology*, 205(19):4480–4494, 2011. DOI: 10.1016/j.surfcoat.2011.03.080.

[32] S. Bagherifard, R. Ghelichi, and M. Guagliano. On the shot peening surface coverage and its assessment by means of finite element simulation: A critical review and some original developments. *Applied Surface Science*, 259:186–194, 2012. DOI: 10.1016/j.apsusc.2012.07.017.

[33] Y.C. Yen, P. Sartkulvanich, and T. Altan. Finite element modeling of roller burnishing process. *CIRP Annals – Manufacturing Technology*, 54(1):237–240, 2005.

[34] P. Sartkulvanich, T. Altan, F. Jasso, and C. Rodriguez. Finite element modeling of hard roller burnishing: An analysis on the effects of process parameters upon surface finish and residual stresses. *Journal of Manufacturing Science and Engineering, Transactions of the ASME*, 129(4):705–716, 2007. DOI: 10.1115/1.2738121.

[35] W. Bouzid, O. Tsoumarev, and K. Saï. An investigation of surface roughness of burnished aisi 1042 steel. *International Journal of Advanced Manufacturing Technology*, 24(1-2):120–125, 2004. DOI: 10.1007/s00170-003-1761-4.

[36] W. Bouzid and K. Saï. Finite element modeling of burnishing of AISI 1042 steel. *The International Journal of Advanced Manufacturing Technology*, 25(5–6):460–465, 2005. DOI: 10.1007/s00170-003-1993-3.

[37] F. Klocke, V. Bäcker, H. Wegner, and A. Timmer. Innovative FE–Analysis of the Roller Burnishing Process for Different Geometries. In *X International Conference on Computational Plasticity, COMPLAS X*, 2009.

[38] F. Klocke, V. Bäcker, H. Wegner, B. Feldhaus, H.-U. Baron, and R. Hessert. Influence of process and geometry parameters on the surface layer state after roller burnishing of IN718. *Production Engineering*, 3(4–5):391–399, 2009. DOI: 10.1007/s11740-009-0182-0.

[39] P. Balland, L. Tabourot, F. Degre, and V. Moreau. Mechanics of the burnishing process. *Precision Engineering*, 37(1):129–134, 2013. DOI: 10.1016/j.precisioneng.2012.07.008.

[40] Y. Tian and Y.C. Shin. Laser-assisted burnishing of metals. *International Journal of Machine Tools & Manufacture*, 47(1):14–22, 2007. DOI: 10.1016/j.ijmachtools.2006.03.002.

[41] F.-J. Shiou and C.-H. Chuang. Precision surface finish of the mold steel PDS5 using an innovative ball burnishing tool embedded with a load cell. *Precision Engineering*, 34(1):76–84, 2010. DOI: 10.1016/j.precisioneng.2009.03.003.

[42] J. Lu. *Handbook of Measurement of Residual Stresses*. Society for Experimental Mechanics, 1996. Fairmont Press.

[43] BS EN 15305:2008. Non-destructive Testing - Test Method for Residual Stress analysis by X-ray Diffraction. ISBN: 978 0 580 66870 8.

[44] P.S. Prevéy. *X-Ray Diffraction Residual Stress Techniques*. Lambda Research, Inc. Metals Handbook. 10. Metals Park: American Society for Metals, 1986, 380–392.

[45] P.S. Prevéy. *Current Applications of X-Ray Diffraction Residual Stress Measurement*. Lambda Research, Inc. ASM International, Materials Park, OH, 1996, pp 103–110.

[46] M. Beghini, L. Bertini, and L.F. Mori. Evaluating non-uniform residual stress by the hole-drilling method with concentric and

eccentric holes. Part I. Definition and validation of the influence functions. *Strain*, 46(4):324–336, 2010. DOI: 10.1111/j.1475-1305.2009.00683.x.

[47] M. Beghini, L. Bertini, and L.F. Mori. Evaluating non-uniform residual stress by the hole-drilling method with concentric and eccentric holes. Part II: Application of the influence functions to the inverse problem. *Strain*, 46(4):337–346, 2010. DOI: 10.1111/j.1475-1305.2009.00684.x.

[48] M. Beghini, L. Bertini, and C. Santus. A procedure for evaluating high residual stresses using the blind hole drilling method, including the effect of plasticity. *Journal of Strain Analysis for Engineering Design*, 45(4):301–318, 2010. DOI: 10.1243/03093247JSA579.

[49] M. Beghini, C. Santus, E. Valentini, and A. Benincasa. Experimental verification of the hole drilling plasticity effect correction. *Materials Science Forum*, 681:151–158, 2011. DOI: 10.4028/www.scientific.net/MSF.681.151.

[50] P.V. Grant, P.D. Lord, and P.S. Whitehead. *The Measurement of Residual Stresses by the Incremental Hole Drilling Technique*. National Physical Laboratory, Teddington, Middlesex, UK, 2002. Measurement good practice guide No. 53.

[51] E. Valentini, M. Beghini, L. Bertini, C. Santus, and M. Benedetti. Procedure to perform a validated incremental hole drilling measurement: Application to shot peening residual stresses. *Strain*, 47(Suppl. 1):e605–e618, 2011. DOI: 10.1111/j.1475-1305.2009.00664.x.

[52] E. Valentini, A. Benincasa, and C. Santus. Bending test rig for validating the hole drilling method residual stress measurement. *Materials Science Forum*, 768–769:150–157, 2014. DOI: 10.4028/www.scientific.net/MSF.768-769.150.

[53] P.V. Grant. *Evaluation of Residual Stress Measurement Uncertainties using X-Ray Diffraction and Hole Drilling via a UK Intercomparison Exercise*. National Physical Laboratory, Teddington, Middlesex, UK, 2002. MATC(MN)020.

[54] V. Fontanari, F. Frendo, T. Bortolamedi, and P. Scardi. Comparison of the hole-drilling and X-ray diffraction methods for measuring the residual stresses in shot-peened aluminium alloys. *Journal of Strain Analysis for Engineering Design*, 40(2):199–209, 2005. DOI: 10.1243/030932405X7791.

[55] N.S. Rossini, M. Dassisti, K.Y. Benyounis, and A.G. Olabi. Methods of measuring residual stresses in components. *Materials and Design*, 35:572–588, 2012. DOI: 10.1016/j.matdes.2011.08.022.

[56] M. Bijak-Żochowski and P. Marek. Residual stress in some elasto-plastic problems of rolling contact with friction. *International Journal of Mechanical Sciences*, 39(1):15–32, 1997.

[57] W.Z. Zhuang and G.R. Halford. Investigation of residual stress relaxation under cyclic load. *International Journal of Fatigue*, 23(Suppl. 1):31–37, 2001. DOI: 10.1016/S0142-1123(01)00132-3.

[58] R. Avilés, J. Albizuri, A. Rodríguez, and L.N. López de Lacalle. Influence of low-plasticity ball burnishing on the high-cycle fatigue strength of medium carbon AISI 1045 steel. *International Journal of Fatigue*, 55:230–244, 2013. DOI: 10.1016/j.ijfatigue.2013.06.024.

[59] G.H. Majzoobi, K. Azadikhah, and J. Nemati. The effects of deep rolling and shot peening on fretting fatigue resistance of aluminum-7075-t6. *Materials Science and Engineering A*, 516(1–2):235–247, 2009. DOI: 10.1016/j.msea.2009.03.020.

List of Figures

List of Tables

All the figures (.eps format) are uploaded along with the LaTeX source files attached to this submission.